

Noise-Resistant Quantum State Compression Readout

Chen Ding,¹ Yun-Fei Niu,¹ Wan-Su Bao,^{1,*} and He-Liang Huang^{1, 2, 3, †}

¹*Henan Key Laboratory of Quantum Information and Cryptography, Zhengzhou, Henan 450000, China*

²*Hefei National Laboratory for Physical Sciences at Microscale and Department of Modern Physics, University of Science and Technology of China, Hefei, Anhui 230026, China*

³*Shanghai Branch, CAS Centre for Excellence and Synergetic Innovation Centre in Quantum Information and Quantum Physics, University of Science and Technology of China, Hefei, Anhui 201315, China*

(Dated: November 2, 2021)

Qubit measurement is generally the most error-prone operation that degrades the performance of near-term quantum devices, and the exponential decay of readout fidelity seriously impedes the development of large-scale quantum information processing. In light of this, we present a quantum state readout method, named *compression readout*, that naturally avoids large multi-qubit measurement error, by compressing the quantum state into a single qubit for measurement. Our method outperforms direct measurements on accuracy as it reduces the decay rate of readout fidelity, and hence has an advantage that grows with the system size, conditioned on readout error moderately greater than gate error. Moreover, since only one-qubit measurements are performed, our method requires solely a fine readout calibration on one qubit and is free of correlated measurement error, which drastically diminishes the demand for device calibration. These advantages suggest our method can boost the readout performance of near-term quantum devices immediately, and will greatly benefit the development towards large-scale quantum computing.

Introduction.—The physical implementations of quantum computing have developed tremendously [1–14]. In particular, the milestone of quantum computational advantage (also known as *quantum supremacy*) has been reached using superconducting and optical systems [2–4, 15], which marks a tendency of accelerating development in quantum computing. Nowadays, with the capacity of implementing the near-term quantum computing applications, such as quantum machine learning [16–22], cloud quantum computing [23–27], and quantum simulation [28–34], we have stepped into the Noisy Intermediate-Scale Quantum (NISQ) era.

Several hurdles must be solved before quantum computing becomes widespread and reaches its full potential. Maintaining high-fidelity quantum operations while increasing the number of qubits is the main task of current quantum computing. To run large applications, the sources of noise, including gate error, readout error, decoherence and cross-talk, must be carefully suppressed. Take the state-of-the-art quantum processor *Zuchongzhi* [4] as an example, the final fidelity of random quantum circuit with 60-qubit and 20-cycle is only 0.0672%, although the quantum operation has reached a high fidelity (Single-qubit gate error is 0.14%, two-qubit gate error is 0.59%, and readout error is 4.52%). Moreover, we can find that the readout error is an order of magnitude higher than the gate error, which is the main error of this processor. Considering that the fidelity exponentially decay as the number of qubits grows, and readout is inevitable in quantum computing for obtaining results, reducing readout error is essential for large-scale quantum computing implementation.

Currently, the main methods for suppressing readout error are the transition matrix error mitigation method

(TMEM) and its variations [35–38], which involve applying an inverse noise matrix (yielded by the device calibration data) to the direct measurement outcome, along with other methods such as measurement subsetting[39], and Invert-and-Measure[40]. The mitigation methods are most effective, as they may suppress most of the readout error once the device is well-calibrated. However, as the system size grows, many issues show up for error mitigation methods, such as: (i) Mitigating correlated readout error brings an exponential time overhead for calibration or mitigation [37]. (ii) The calibration error accumulates as the system size grows. (iii) The stability of the whole physical system is hard to maintain during the large-size calibration.

In this paper, we propose a quantum state readout method to avoid the large readout noise in multi-qubit measurements. The method *compresses* the quantum state into one qubit, and read the state from one-qubit measurement results. The compression is implemented by introducing an ancillary qubit, and encoding the information of the amplitudes of the original quantum state to this ancillary qubit through several controlled rotation operations. After performing measurement on this ancillary qubit, only a classical decoding operation is required to recover the amplitudes information of the quantum state. As a result, the task of measuring a multi-qubit state is reduced to a single-qubit readout, and the issue of readout fidelity exponentially decaying with the number of qubits is alleviated by lowering the decay rate, conditioned on measurement error is moderately greater than gate error on the quantum device. Since large-scale readout calibration is no more needed (only the one qubit to be measured needs to be fine calibrated), the problems of mitigation methods as mentioned above are nat-

urally avoided. We provide theoretical analysis for proof of its advantage over direct measurements and numerical experiments for showing its practicality in large-scale quantum state readout.

Method.—Given copies of n -qubit quantum state $|\psi\rangle = \sum_{i=0}^{2^n-1} \alpha_i |i\rangle$, the compression readout algorithm first encodes the information of amplitudes α_i into an ancilla qubit through a special controlled rotation scheme, so that the probability of the ancilla qubit being $|0\rangle$ is a Fourier series with α_i as coefficients. Then we measure this ancilla qubit to estimate the $|0\rangle$ probability. Finally, we recover all $|\alpha_i|^2$ according to a trapezoidal rule for discrete integration of the Fourier series. The specific steps are as follows (see Fig. 1):

Step 1. Initialization. Given accuracy ϵ and success probability $1 - \eta$, Take the grid density m as $2^n - 1$ and the number of measurement shots on each grid point as

$$N = \frac{48m^2 + 4m(2m+1)\epsilon}{(2m+1)^2\epsilon^2} \log\left(\frac{m}{\eta}\right). \quad (1)$$

Set integration grid values x_1, \dots, x_m as $x_k = \frac{k}{2m+1}\pi$ for $k = 1, \dots, m$.

Step 2. Encoding. For k in $\{1, \dots, m\}$, do the following:

(i) Introduce an ancilla qubit $|0\rangle$, perform the controlled rotation operation on $|\psi\rangle|0\rangle$, as

$$|\psi\rangle|0\rangle \rightarrow \sum_{i=0}^{2^n-1} \alpha_i (\cos ix_k |i\rangle|0\rangle + \sin ix_k |i\rangle|1\rangle). \quad (2)$$

The corresponding circuit is shown in the lower left corner of Fig. 1.

(ii) Measure the ancilla qubit in the computational basis for N shots, yield $\tilde{A}(x_k)$ as the estimation of $A(x_k)$, the $|0\rangle$ probability.

Step 3. Decoding. Calculate the estimate of $|\alpha_i|^2$ as

$$p_0 \leftarrow \frac{1}{2m+1} \left(1 - 2m + 4 \sum_{k=1}^m \tilde{A}(x_k) \right), \quad (3)$$

$$p_{i \neq 0} \leftarrow \frac{4}{2m+1} \left(1 + 2 \sum_{k=1}^m \tilde{A}(x_k) \cos 2ix_k \right). \quad (4)$$

To make the algorithm more concrete, we show its pseudocode as follows:

Algorithm 1 The Quantum State Compression Readout

Input: Multiple quantum states $|\psi\rangle = \sum_{i=0}^{2^n-1} \alpha_i |i\rangle$. Preset accuracy ϵ and success probability $1 - \eta$.

Goal: Output the squared modulus of the amplitudes in $|\psi\rangle$, namely $|\alpha_i|^2$.

Init: Set $m = 2^n - 1$. Set N as Formula (1). Set grid values x_1, \dots, x_m as $x_k = \frac{k}{2m+1}\pi$, $k = 1, \dots, m$.

for $k = 1 : m$ **do**

$\tilde{A}(x_k) \leftarrow 0$.

for $l = 1 : N$ **do**

 Append $|\psi\rangle$ with an ancilla qubit $|0\rangle$.

 Do controlled rotation on $|\psi\rangle|0\rangle$ as Formula (2).

 Measure the ancilla qubit in the computational basis. If yielding $|0\rangle$, $\tilde{A}(x_k) \leftarrow \tilde{A}(x_k) + \frac{1}{N}$.

end for

end for

for $i = 0 : 2^n - 1$ **do**

 Set p_i as Formula (3,4).

end for

Output: p_i for $i = 0, \dots, 2^n - 1$.

We put here a theorem stating the correctness of our algorithm and the basic idea of proving it. See Supplemental Material for its rigorous proof.

Theorem 1 (Correctness). *Given the a n -qubit quantum state $|\psi\rangle = \sum_{i=0}^{2^n-1} \alpha_i |i\rangle$, when setting the number of grid density $m = 2^n - 1$ and the number of shots on each grid point as Formula (1), Algorithm 1 yields approximation of all the squared modulus of the amplitudes with accuracy ϵ , success probability at least $1 - \eta$. In other words, $\forall i = 0, \dots, 2^n - 1$,*

$$\mathbb{P}(|p_i - |\alpha_i|^2| \geq \epsilon) \leq \eta,$$

in which p_i are the approximation values.

The correctness of the algorithm can be roughly understood in this way. After the controlled rotation in Step 2, the probability of yielding $|0\rangle$ in the ancilla qubit is

$$A = \sum_{i=0}^{2^n-1} |\alpha_i|^2 \cos^2 ix \quad (5)$$

$$= \frac{1}{2}(1 + |\alpha_0|^2) + \frac{1}{2} \sum_{i=1}^{2^n-1} |\alpha_i|^2 \cos 2ix \quad (6)$$

$$=: A(x), \quad (7)$$

which is a Fourier series with variable x . We can recover its coefficients $|\alpha_i|^2$ by inverse Fourier transform:

$$|\alpha_i|^2 = \begin{cases} \frac{4}{\pi} \int_0^\pi A(x) dx - 1, & i = 0, \\ \frac{4}{\pi} \int_0^\pi A(x) \cos 2ix dx, & i \neq 0. \end{cases}$$

We use a trapezoidal rule to calculate this integration. Since the integrated function $A(x) \cos 2ix$ is even on both endpoints of $[0, \pi]$, the sum converges exponentially fast over m [41]:

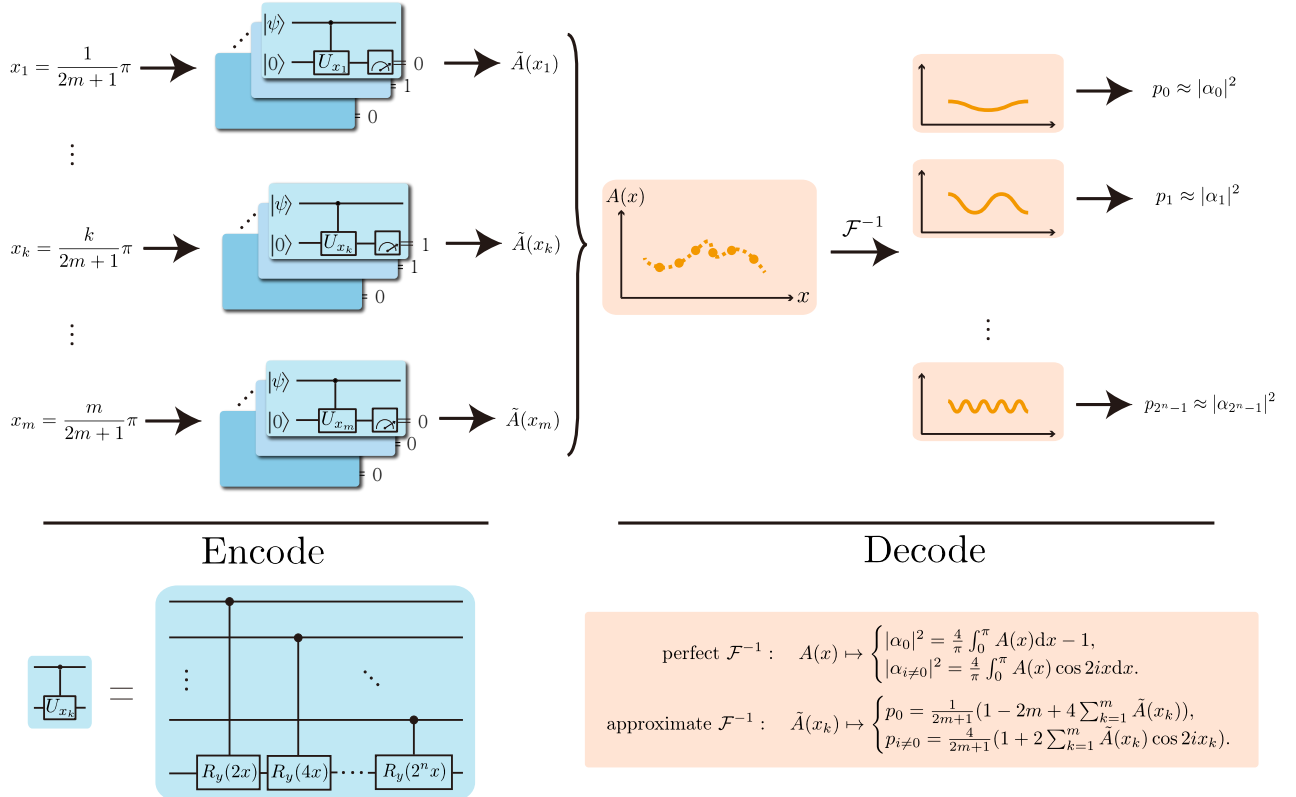


FIG. 1: **The schematic diagram of compression readout method.** The algorithm include two stages: encode and decode. In the encode stage, we do batches of controlled rotation for quantum state $|\psi\rangle|0\rangle$ and measure the ancilla qubit, yielding estimations for the Fourier series $A(x)$ as $\tilde{A}(x_k)$. The encoding controlled rotation can be implemented using only n two-qubit gates, as shown in the lower left corner. In the decode stage, we recover the squared modulus of the amplitudes of $|\psi\rangle$ through inverse Fourier transform on the array of $\tilde{A}(x_k)$.

$$|\alpha_0|^2 = \frac{1}{2m+1} \left(1 - 2m + 4 \sum_{k=1}^m \tilde{A}(x_k) \right) + O(e^{-m}), \quad (8)$$

$$|\alpha_i|^2 = \frac{4}{2m+1} \left(1 + 2 \sum_{k=1}^m \tilde{A}(x_k) \cos 2ix_k \right) + O(e^{-m}), \quad (9)$$

in which the integration grid points are $x_k = \frac{k}{2m+1}\pi$, $k = 1, \dots, m$. By replacing the theoretical probabilities $A(x_k)$ with its realistic estimation $\tilde{A}(x_k)$ and ignore the last item, we yield the formula of $|\alpha_i|^2$ same as Formula (3,4). Therefore, with the techniques above, we can recover the squared modulus of the amplitudes of $|\psi\rangle$. We show the last item $O(e^{-m})$ in Equation (8,9) equals 0 when $m \geq 2^n - 1$ in proof of Theorem 1.

Theoretical comparison with direct readout.—To show the accuracy and noise-resistance capability of the compression readout algorithm, we compared it to a conventional plain readout method—direct readout. Given

multiple copies of $|\psi\rangle$, direct readout method measures them in the computational basis for M shots to obtain the frequencies of each basis state, namely q_i . As long as M is large enough, these frequencies are good estimators of $|\alpha_i|^2$. For the sake of comparison, we also provide the pseudo code of this conventional method in Alg. 2.

Algorithm 2 The Direct Quantum State Readout

Input: Multiple quantum states $|\psi\rangle = \sum_{i=0}^{2^n-1} \alpha_i |i\rangle$. Preset accuracy ϵ and success probability $1 - \eta$.

Goal: Output the squared modulus of the amplitudes in $|\psi\rangle$, namely $|\alpha_i|^2$.

Init: Set $M = \frac{3+\epsilon}{\epsilon^2} \log(\frac{1}{\eta})$.

for $i = 1 : 2^n$ **do**

$q_i \leftarrow 0$.

end for

for $l = 1 : M$ **do**

For a copy of quantum state $|\psi\rangle$, measure it in the computational basis. If yielding i , $q_i \leftarrow q_i + \frac{1}{M}$.

end for

Output: q_i for $i = 0, \dots, 2^n - 1$.

To make a fair comparison between compression readout and direct readout, we let N be a constant, and make

the total measurement shots of the two methods equals, i.e., $M = mN = (2^n - 1)N$. We compare the compression readout to direct readout in two scenarios: The noise-free case and the noisy case.

(i) **Scenario I: The noise-free case.** We first consider the case that all operations are free of noise and show our method is comparable to direct readout on the statistical stability of outcomes.

In this situation, the outputs of the two algorithms are unbiased estimation for $|\alpha_i|^2$. To measure their statistical stability, we calculate the variance:

$$D(p_i) = \mathbb{E}[(p_i - \mathbb{E}p_i)^2],$$

for the compression readout method and

$$D(q_i) = \mathbb{E}[(q_i - \mathbb{E}q_i)^2],$$

for the direct readout method.

Those variances reflect how the estimators deviate from their expectation values $|\alpha_i|^2$ due to statistical error in measurements.

In the compression readout method, since $\tilde{A}(x_k)$ is the estimation of the probability of $|0\rangle$ in the ancilla qubit, we have

$$\tilde{A}(x_k) = \frac{\sum_{j=1}^N X_j^{(k)}}{N},$$

in which $X_j^{(k)}$ are the random variables in each shot, satisfying a binary distribution as

$$\begin{aligned} \mathbb{P}(X_j^{(k)} = 1) &= A(x_k) \\ &= \frac{1}{2} + \frac{1}{2} \sum_{i=0}^{2^n-1} |\alpha_i|^2 \cos 2ix_k. \end{aligned}$$

According to the formula of $\tilde{A}(x_k)$, we have

$$\begin{aligned} D(\tilde{A}(x_k)) &= \frac{A(x_k)(1 - A(x_k))}{N} \\ &= \frac{1}{N} \left(1 - \left(\sum_{j=0}^{2^n-1} |\alpha_j|^2 \cos 2jx_k \right)^2 \right) \\ &\leq \frac{1}{N}. \end{aligned}$$

Thus

$$\begin{aligned} D(p_0) &= \frac{16}{(2m+1)^2} \sum_{k=1}^m D(\tilde{A}(x_k)) \\ &\leq \frac{16m}{(2m+1)^2 N}. \end{aligned}$$

For $i \neq 0$,

$$\begin{aligned} D(p_i) &= \frac{64}{(2m+1)^2} \sum_{k=1}^m D(\tilde{A}(x_k)) \cos^2 2ix_k \\ &\leq \frac{64}{(2m+1)^2 N} \sum_{k=1}^m \cos^2 2ix_k \\ &\leq \frac{32}{(2m+1)^2 N} \sum_{k=1}^m (\cos 4ix_k + 1) \\ &= \frac{16}{(2m+1)^2 N}. \end{aligned}$$

Thus $\forall i \in \{0, \dots, 2^n - 1\}$,

$$D(p_i) \leq \frac{16m}{(2m+1)^2 N}.$$

For direct readout, since we do mN shots of measurement, we have

$$q_i = \frac{\sum_{j=1}^{mN} Y_j^{(i)}}{mN},$$

in which $Y_j^{(i)}$ are the random variables in each shot, satisfying a binary distribution as

$$\mathbb{P}(Y_j^{(i)} = 1) = |\alpha_i|^2.$$

Thus the variances of q_i is

$$D(q_i) = \frac{|\alpha_i|^2(1 - |\alpha_i|^2)}{mN}.$$

Since

$$\begin{aligned} \frac{D(p_i)}{D(q_i)} &\leq \frac{16m^2}{(2m+1)^2 |\alpha_i|^2(1 - |\alpha_i|^2)} \\ &\leq \frac{16}{|\alpha_i|^2(1 - |\alpha_i|^2)} \end{aligned}$$

when $|\alpha_i|^2 = O(1)$, the ratio of variance $D(p_i)$ and $D(q_i)$ is bounded by a constant. This fact shows when the number of qubits or measurement shots increases, the variances of Alg. 1 will not grow faster than variances of Alg. 2, which means Alg. 1 is comparable to Alg. 2 in the noise-free case.

(ii) **Scenario II: The noisy case.** We then consider the case where quantum gates are imperfect, and readout error occurs. We show compression readout outperforms direct readout on accuracy in this case.

For convenience of analysis, we simplify the error model as follows: First, we adopt an independent symmetric bit flip channel for each qubit as the readout noise, which is commonly used in readout noise analysis and mitigation[36, 42]: During each shot in the measurement, the readout result of each qubit has a probability ξ of flipping its value ($|0\rangle$ goes to $|1\rangle$ and $|1\rangle$ goes to $|0\rangle$). Then,

we suppose each gate in compression readout has fidelity γ .

To grasp the benefits of compression readout intuitively, we first do a rough sketch of the readout fidelities of the two methods using the simple model in [2]. The fidelities of compression readout and direct readout can be estimated from a simple multiplication of individual gate fidelities and measurement fidelities as

$$F_{\text{direct}} = (1 - \xi)^n,$$

$$F_{\text{compression}} = (1 - \gamma)^n(1 - \xi).$$

We find both fidelities decrease minus exponentially with the system size n . However, the compression readout has an exponential advantage in the case of the readout error is greater than the gate error, making compression readout very suitable for state-of-the-art processors, such as Sycamore [2] and *Zuchongzhi* [4].

Next, we provide a rigorous analysis for the advantage of compression readout based on the algorithm flow and the error model. We compare the expected total deviations of the two algorithms, which are

$$B_1 := \sum_{i=0}^{2^n-1} |\mathbb{E}p_i - |\alpha_i|^2|,$$

for the compression readout method and

$$B_2 := \sum_{i=0}^{2^n-1} |\mathbb{E}q_i - |\alpha_i|^2|,$$

for the direct readout method. As ℓ_1 distance between the algorithm's realistic output and the readout target $(|\alpha_i|^2)_{i=0, \dots, 2^n-1}$, the expected total deviations are naturally the measure of algorithm accuracy.

Suppose the theoretical outcome state after the controlled rotation in compression readout is ρ , and the outcome with imperfect gates is σ . Since there are n gates in the circuit, the fidelity between ρ and σ can be estimated as $F(\rho, \sigma) = (1 - \gamma)^n$. And the bias of the probability of $|0\rangle$ in the ancilla qubit is

$$\begin{aligned} \Delta_k &= |A(x_k) - A(x_k)_{\text{imperfect gates}}| \\ &\leq 2T(\rho_A, \sigma_A) \\ &\leq 2T(\rho, \sigma) \\ &\leq 2\sqrt{1 - F(\rho, \sigma)} \\ &= 2\sqrt{1 - (1 - \gamma)^n}, \end{aligned}$$

in which $T(\cdot, \cdot)$ is the trace distance, ρ_A and σ_A are the reduced density matrices in the subsystem of the one ancilla qubit.

Considering readout error, the realistic estimation of the probability of $|0\rangle$ in the ancilla qubit $\tilde{A}(x_k)$ will be

$$\begin{aligned} \mathbb{E}\tilde{A}(x_k) &= (1 - \xi)(A(x_k) \pm \Delta_k) + \xi(1 - A(x_k) \mp \Delta_k) \\ &= A(x_k) + \xi - 2\xi A(x_k) \pm (1 - 2\xi)\Delta_k. \end{aligned}$$

From Formula (3,4), we yield

$$\begin{aligned} \mathbb{E}p_0 &= \frac{1}{2m+1} \left(1 - 2m + 4 \sum_{k=1}^m \mathbb{E}\tilde{A}(x_k) \right) \\ &= \frac{1}{2m+1} (1 - 2m + 4 \sum_{k=1}^m (A(x_k) + \xi - 2\xi A(x_k) \pm (1 - 2\xi)\Delta_k)) \\ &= (1 - 2\xi)|\alpha_0|^2 + \frac{2\xi}{2m+1} + \frac{4(1 - 2\xi)}{2m+1} \sum_{k=1}^m (\pm \Delta_k), \end{aligned}$$

$$\begin{aligned} \mathbb{E}p_{i \neq 0} &= \frac{4}{2m+1} \left(1 + 2 \sum_{k=1}^m \mathbb{E}\tilde{A}(x_k) \cos 2ix_k \right) \\ &= \frac{4}{2m+1} (1 + 2 \sum_{k=1}^m (A(x_k) + \xi - 2\xi A(x_k) \pm (1 - 2\xi)\Delta_k) \cos 2ix_k) \\ &= (1 - 2\xi)|\alpha_i|^2 + \frac{8(1 - 2\xi)}{2m+1} \sum_{k=1}^m (\pm \Delta_k \cos 2ix_k). \end{aligned}$$

Assuming the system size n is large, we use the $O(\cdot)$ notation to analyze the limiting behavior of B_1 .

$$\begin{aligned} B_1 &= \sum_{i=0}^{2^n-1} |\mathbb{E}p_i - |\alpha_i|^2| \\ &= \left| -2\xi|\alpha_0|^2 + \frac{2\xi}{2m+1} + O((1 - 2\xi)\sqrt{1 - (1 - \gamma)^n}) \right| \\ &\quad + \sum_{i=1}^{2^n-1} \left| 2\xi|\alpha_i|^2 + O\left(\frac{1 - 2\xi}{m}\sqrt{1 - (1 - \gamma)^n}\right) \right| \\ &= O(\xi|\alpha_0|^2 + (1 - 2\xi)\sqrt{1 - (1 - \gamma)^n}) \\ &\quad + \sum_{i=1}^{2^n-1} O\left(\xi|\alpha_i|^2 + \frac{1 - 2\xi}{m}\sqrt{1 - (1 - \gamma)^n}\right) \\ &= O(\xi + (1 - 2\xi)\sqrt{1 - (1 - \gamma)^n}). \end{aligned}$$

For direct readout, we give the following theorem (see proof in the Supplemental Material).

Theorem 2 (the total deviation of direct readout). *For a n -qubit quantum state $|\psi\rangle = \sum_{i=0}^{2^n-1} \alpha_i |i\rangle$ randomly sampled from Haar distribution, the total deviation of direct readout is larger than a minus exponential function of n with probability one. In other words,*

$$B_2 \geq C(1 - (1 - 2\xi)^n),$$

in which

$$C = \left| \frac{\sum_{i=0}^{2^n-1} (-1)^{\sum i_j} |\alpha_i|^2}{2^{\frac{n}{2}}} \right|$$

is a constant depending on the state and $\mathbb{P}(C > 0) = 1$. (i_j is the j -th number of the binary representation of index i).

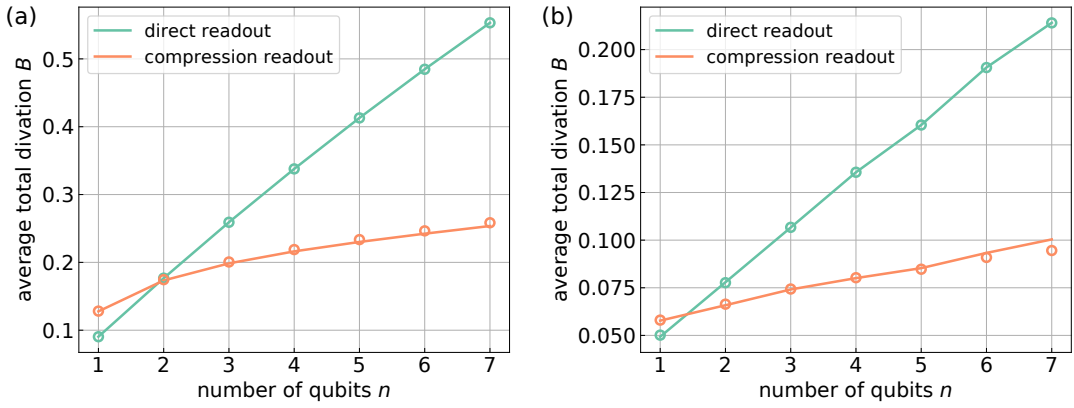


FIG. 2: The average total deviations of the compression readout algorithm and direct readout with increasing numbers of qubits. (a) and (b) are the results for the zero state $|0\dots0\rangle$ and random quantum states sampled from Haar distribution, respectively. Each data points on the lines is an average total deviation over 100 numerical experiments, and the circles are our estimation of total deviations, calculated by multiplying density matrices. All the numerical simulations are implemented in the settings of measurement shot $N = 100000$, readout error $\xi = 0.0452$, depolarizing probability $\gamma = 0.0059$, and grid density $m = 2^n - 1$.

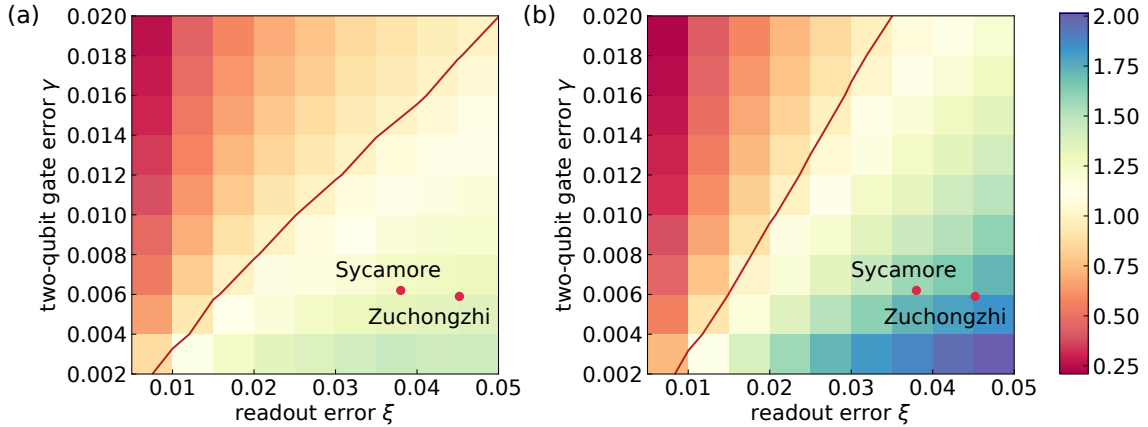


FIG. 3: The heatmap of the ratio of the deviation between compression readout and direct readout as a function of readout error and gate error. Each square shows the ratio of average total deviations (B_2/B_1) over 100 experiments. The experiment settings are: Readout error $\xi \in \{0.005, \dots, 0.05\}$, depolarizing probability $\gamma \in \{0.002, \dots, 0.02\}$, measurement shot $N = 1000$, and grid density $m = 2^n - 1$. (a) and (b) are the results for three-qubit state $|000\rangle$ and six-qubit state $|000000\rangle$, respectively. The red contour lines show the noise combination where the ratio equals 1. The area under the line is where the compression readout shows its advantage. We also mark the two-qubit gate error and readout error of the state-of-the-art quantum processors Sycamore [2] and Zuchongzhi [4] in the heatmap.

By subtracting half of the modulus square of amplitudes from another half of them, C represents some type of *balance* measure for the quantum state. Reading a balanced state may lead to less deviations, e.g., $B_2 = 0$ for a uniform state $\frac{1}{\sqrt{2^n}} \sum_{i=0}^{2^n-1} |i\rangle$. However, generally the total deviation B_2 of direct readout grows with system size at the rate of ξ .

From the formula of B_1 and Theorem 2, we find total deviation B_2 of direct readout is asymptotically larger than B_1 of compression readout. Therefore, compression readout is advantageous for reducing measurement error on large systems, conditioned on a positive difference of the readout error ξ and the gate error γ . We note that our

analysis for the total deviations focuses on their limiting behavior, and is not tight enough. We further validate our analysis with numerical experiments, and explore the practical advantageous area for compression readout.

Numerical Experiments—We simulate the compression readout and direct readout using Qiskit[43] to compare their performance under simulated noise. To simulate gate error in the compression readout algorithm’s circuit, we add a two-qubit depolarization channel of depolarizing probability γ after each precise controlled- R_y gate in our program. And we add an independent symmetric bit flip channel (as introduced in theoretical analysis) for each shot of measurements.

Figure 2 shows the average total deviations of the compression readout and direct readout with increasing numbers of qubits for the state $|0\dots0\rangle$ and random quantum states. In our simulation, the readout error ξ and depolarizing probability γ are set as $\xi = 0.0452$ and $\gamma = 0.0059$, respectively, as a rough imitation of the state-of-the-art quantum processor *Zuchongzhi* [4]. The deviations of these two methods increase with the growth of system size, due to the accumulation of readout and gate errors, while the compression readout is obviously more robust against the expansion of the number of qubits. Another phenomenon is that the total deviation of reading random quantum states is lower than reading the zero states $|0\dots0\rangle$, which is mainly due to the readout noise causing interchanges of probability among all the measurement results. As mentioned in our theoretical analysis, a random state is more *balanced* than a zero state.

In the Fig. 3, we show the ratio of the deviation between compression readout and direct readout, as a function of readout error and gate error. Generally the compression readout algorithm outperforms direct readout when the readout error is high and gate error is low, since it avoids large-scale measurements at the cost of extra gates. In fact, for the state-of-the-art processors Sycamore [2] and *Zuchongzhi* [4] processors, the readout error is an order of magnitude higher than the gate error. Thus, the performance of current noisy quantum devices could be boosted immediately by the compression readout. As shown in Fig. 3, the red points that represent the operations' noise on Sycamore [2] and *Zuchongzhi* [4] processors are all in the dominant region of compression readout. Furthermore, the dominant region of compression readout expands rapidly when number of qubits n increases, in consistency with the phenomena in Fig. 2, and also shows that compression readout is well suited to large-scale quantum state readout.

Conclusion—Our proposed quantum state compression readout method is resistant to the huge noise caused by multi-qubit measurement, by encoding the information-to-read into one qubit. The method improves the accuracy of reading quantum states without adding extra measurement shots, and can naturally overcome the problems of mitigating correlated error and large-scale calibration. The compression readout has obvious noise-resistance effect on current noisy state-of-the-art quantum devices, such as Sycamore [2] and *Zuchongzhi* [4] processors. And the advantage expands rapidly as the system size increases, making the compression readout a promising alternative method for high-fidelity large-scale quantum state readout. By enhancing the integration scheme and combining with error mitigation schemes, the compression readout method might be enhanced even further.

H.-L. H. acknowledges support from the Youth Talent Lifting Project (Grant No. 2020-JCJQ-QT-030), Na-

tional Natural Science Foundation of China (Grants No. 11905294), China Postdoctoral Science Foundation, and the Open Research Fund from State Key Laboratory of High Performance Computing of China (Grant No. 201901-01).

* bws@qiclab.cn

† quanhhl@ustc.edu.cn

- [1] H.-L. Huang, D. Wu, D. Fan, and X. Zhu, *Sci. China Inf. Sci.* **63**, 180501 (2020).
- [2] F. Arute, K. Arya, R. Babbush, D. Bacon, J. C. Bardin, R. Barends, R. Biswas, S. Boixo, F. G. S. L. Brandao, D. A. Buell, B. Burkett, Y. Chen, Z. Chen, B. Chiaro, R. Collins, W. Courtney, A. Dunsworth, E. Farhi, B. Foxen, A. Fowler, C. Gidney, M. Giustina, R. Graff, K. Guerin, S. Habegger, M. P. Harrigan, M. J. Hartmann, A. Ho, M. Hoffmann, T. Huang, T. S. Humble, S. V. Isakov, E. Jeffrey, Z. Jiang, D. Kafri, K. Kechedzhi, J. Kelly, P. V. Klimov, S. Knysh, A. Korotkov, F. Kostritsa, D. Landhuis, M. Lindmark, E. Lucero, D. Lyakh, S. Mandrà, J. R. McClean, M. McEwen, A. Megrant, X. Mi, K. Michelsen, M. Mohseni, J. Mutus, O. Naaman, M. Neeley, C. Neill, M. Y. Niu, E. Ostby, A. Petukhov, J. C. Platt, C. Quintana, E. G. Rieffel, P. Roushan, N. C. Rubin, D. Sank, K. J. Satzinger, V. Smelyanskiy, K. J. Sung, M. D. Tervitthick, A. Vainsencher, B. Villalonga, T. White, Z. J. Yao, P. Yeh, A. Zalcman, H. Neven, and J. M. Martinis, *Nature* **574**, 505 (2019).
- [3] H.-S. Zhong, H. Wang, Y.-H. Deng, M.-C. Chen, L.-C. Peng, Y.-H. Luo, J. Qin, D. Wu, X. Ding, Y. Hu, P. Hu, X.-Y. Yang, W.-J. Zhang, H. Li, Y. Li, X. Jiang, L. Gan, G. Yang, L. You, Z. Wang, L. Li, N.-L. Liu, C.-Y. Lu, and J.-W. Pan, *Science* **370**, 1460 (2020).
- [4] Y. Wu, W.-S. Bao, S. Cao, F. Chen, M.-C. Chen, X. Chen, T.-H. Chung, H. Deng, Y. Du, D. Fan, M. Gong, C. Guo, C. Guo, S. Guo, L. Han, L. Hong, H.-L. Huang, Y.-H. Huo, L. Li, N. Li, S. Li, Y. Li, F. Liang, C. Lin, J. Lin, H. Qian, D. Qiao, H. Rong, H. Su, L. Sun, L. Wang, S. Wang, D. Wu, Y. Xu, K. Yan, W. Yang, Y. Yang, Y. Ye, J. Yin, C. Ying, J. Yu, C. Zha, C. Zhang, H. Zhang, K. Zhang, Y. Zhang, H. Zhao, Y. Zhao, L. Zhou, Q. Zhu, C.-Y. Lu, C.-Z. Peng, X. Zhu, and J.-W. Pan, arXiv:2106.14734 (2021).
- [5] P. Jurcevic, A. Javadi-Abhari, L. S. Bishop, I. Lauer, D. F. Bogorin, M. Brink, L. Capelluto, O. Günlük, T. Itoko, N. Kanazawa, A. Kandala, G. A. Keefe, K. Krulich, W. Landers, E. P. Lewandowski, D. T. McClure, G. Nannicini, A. Narasgond, H. M. Nayfeh, E. Pritchett, M. B. Rothwell, S. Srinivasan, N. Sundaresan, C. Wang, K. X. Wei, C. J. Wood, J.-B. Yau, E. J. Zhang, O. E. Dial, J. M. Chow, and J. M. Gambetta, *Quantum Sci. and Technol.* **6**, 025020 (2021).
- [6] J. L. O'Brien, *Science* **318**, 1567 (2007).
- [7] S.-H. Tan and P. P. Rohde, *Rev. Phys.* **4**, 100030 (2019).
- [8] X.-L. Wang, L.-K. Chen, W. Li, H.-L. Huang, C. Liu, C. Chen, Y.-H. Luo, Z.-E. Su, D. Wu, Z.-D. Li, H. Lu, Y. Hu, X. Jiang, C.-Z. Peng, L. Li, N.-L. Liu, Y.-A. Chen, C.-Y. Lu, and J.-W. Pan, *Phys. Rev. Lett.* **117**, 210502 (2016).

[9] X.-L. Wang, Y.-H. Luo, H.-L. Huang, M.-C. Chen, Z.-E. Su, C. Liu, C. Chen, W. Li, Y.-Q. Fang, X. Jiang, J. Zhang, L. Li, N.-L. Liu, C.-Y. Lu, and J.-W. Pan, *Phys. Rev. Lett.* **120**, 260502 (2018).

[10] G. Moody, V. Sorger, P. Juodawlkis, W. Loh, C. Sorace-Agaskar, A. E. Jones, K. Balram, J. Matthews, A. Laing, M. Davanco, L. Chang, J. Bowers, N. Quack, C. Galland, I. Aharonovich, M. Wolff, C. Schuck, N. Sinclair, M. Loncar, T. Komljenovic, D. M. Weld, S. Mookherjea, S. Buckley, M. Radulaski, S. Reitzenstein, G. S. Agarwal, B. Pingault, B. Machielse, D. Mukhopadhyay, A. V. Akiyamov, A. Zheltikov, K. Srinivasan, W. Jiang, T. McKenna, J. Lu, H. Tang, A. H. Safavi-Naeini, S. Steinhauer, A. Elshaari, V. Zwiller, P. Davids, N. Martinez, M. Gehl, J. Chiaverini, K. Mehta, J. Romero, N. Lingaraju, A. M. Weiner, D. Peace, R. Cernansky, M. Lobino, E. Diamanti, R. Camacho, and L. Trigo Vidarte, *J. Phys. Photonics* (2021).

[11] C. Monroe and J. Kim, *Science* **339**, 1164 (2013).

[12] I. Pogorelov, T. Feldker, C. D. Marciniak, L. Postler, G. Jacob, O. Kriegelsteiner, V. Podlesnic, M. Meth, V. Negnevitsky, M. Stadler, B. Höfer, C. Wächter, K. Lakhmanskij, R. Blatt, P. Schindler, and T. Monz, *PRX Quantum* **2**, 020343 (2021).

[13] Y. He, S. K. Gorman, D. Keith, L. Kranz, J. G. Keizer, and M. Y. Simmons, *Nature* **571**, 371 (2019).

[14] S. Ebadi, T. T. Wang, H. Levine, A. Keesling, G. Semeghini, A. Omran, D. Bluvstein, R. Samajdar, H. Pichler, W. W. Ho, S. Choi, S. Sachdev, M. Greiner, V. Vuletić, and M. D. Lukin, *Nature* **595**, 227 (2021).

[15] C. Guo, Y. Zhao, and H.-L. Huang, *Phys. Rev. Lett.* **126**, 070502 (2021).

[16] H.-L. Huang, Y. Du, M. Gong, Y. Zhao, Y. Wu, C. Wang, S. Li, F. Liang, J. Lin, Y. Xu, R. Yang, T. Liu, M.-H. Hsieh, H. Deng, H. Rong, C.-Z. Peng, C.-Y. Lu, Y.-A. Chen, D. Tao, X. Zhu, and J.-W. Pan, *Phys. Rev. Applied* **16**, 024051 (2021).

[17] J. Liu, K. H. Lim, K. L. Wood, W. Huang, C. Guo, and H.-L. Huang, *Sci. China Phys. Mech. Eng.* **64**, 290311 (2021).

[18] H.-L. Huang, X.-L. Wang, P. P. Rohde, Y.-H. Luo, Y.-W. Zhao, C. Liu, L. Li, N.-L. Liu, C.-Y. Lu, and J.-W. Pan, *Optica* **5**, 193 (2018).

[19] M. Schuld and N. Killoran, *Phys. Rev. Lett.* **122**, 040504 (2019).

[20] J. Biamonte, P. Wittek, N. Pancotti, P. Rebentrost, N. Wiebe, and S. Lloyd, *Nature* **549**, 195 (2017).

[21] V. Havlíček, A. D. Córcoles, K. Temme, A. W. Harrow, A. Kandala, J. M. Chow, and J. M. Gambetta, *Nature* **567**, 209 (2019).

[22] V. Saggio, B. E. Asenbeck, A. Hamann, T. Strömberg, P. Schiansky, V. Dunjko, N. Friis, N. C. Harris, M. Hochberg, D. Englund, S. Wölk, H. J. Briegel, and P. Walther, *Nature* **591**, 229 (2021).

[23] S. Barz, E. Kashefi, A. Broadbent, J. F. Fitzsimons, A. Zeilinger, and P. Walther, *Science* **335**, 303 (2012).

[24] H.-L. Huang, Q. Zhao, X. Ma, C. Liu, Z.-E. Su, X.-L. Wang, L. Li, N.-L. Liu, B. C. Sanders, C.-Y. Lu, and J.-W. Pan, *Phys. Rev. Lett.* **119**, 050503 (2017).

[25] H.-L. Huang, W.-S. Bao, T. Li, F.-G. Li, X.-Q. Fu, S. Zhang, H.-L. Zhang, and X. Wang, *Quantum Inf. Process.* **16**, 199 (2017).

[26] H.-L. Huang, Y.-W. Z. nad Tan Li, F.-G. Li, Y.-T. Du, X.-Q. Fu, S. Zhang, X. Wang, and W.-S. Bao, *Front. Phys.* **12**, 120305 (2017).

[27] E. F. Dumitrescu, A. J. McCaskey, G. Hagen, G. R. Jansen, T. D. Morris, T. Papenbrock, R. C. Pooser, D. J. Dean, and P. Lougovski, *Phys. Rev. Lett.* **120**, 210501 (2018).

[28] Y. Cao, J. Romero, J. P. Olson, M. Degroote, P. D. Johnson, M. Kieferová, I. D. Kivlichan, T. Menke, B. Peropadre, N. P. D. Sawaya, S. Sim, L. Veis, and A. Aspuru-Guzik, *Chem. Rev.* **119**, 10856 (2019).

[29] B. Bauer, S. Bravyi, M. Motta, and G. K.-L. Chan, *Chem. Rev.* **120**, 12685 (2020).

[30] S. McArdle, S. Endo, A. Aspuru-Guzik, S. C. Benjamin, and X. Yuan, *Rev. Mod. Phys.* **92**, 015003 (2020).

[31] F. Arute, K. Arya, R. Babbush, D. Bacon, J. C. Bardin, R. Barends, S. Boixo, M. Broughton, B. B. Buckley, D. A. Buell, B. Burkett, N. Bushnell, Y. Chen, Z. Chen, B. Chiaro, R. Collins, W. Courtney, S. Demura, A. Dunsworth, E. Farhi, A. Fowler, B. Foxen, C. Gidney, M. Giustina, R. Graff, S. Habegger, M. P. Harrigan, A. Ho, S. Hong, T. Huang, W. J. Huggins, L. Ioffe, S. V. Isakov, E. Jeffrey, Z. Jiang, C. Jones, D. Kafri, K. Kechedzhi, J. Kelly, S. Kim, P. V. Klimov, A. Korotkov, F. Kostritsa, D. Landhuis, P. Laptev, M. Lindmark, E. Lucero, O. Martin, J. M. Martinis, J. R. McClean, M. McEwen, A. Megrant, X. Mi, M. Mohseni, W. Mruczkiewicz, J. Mutus, O. Naaman, M. Neeley, C. Neill, H. Neven, M. Y. Niu, T. E. O'Brien, E. Ostby, A. Petukhov, H. Putterman, C. Quintana, P. Roushan, N. C. Rubin, D. Sank, K. J. Satzinger, V. Smelyanskiy, D. Strain, K. J. Sung, M. Szalay, T. Y. Takeshita, A. Vainsencher, T. White, N. Wiebe, Z. J. Yao, P. Yeh, and A. Zalcman, *Science* **369**, 1084 (2020).

[32] A. Kandala, A. Mezzacapo, K. Temme, M. Takita, M. Brink, J. M. Chow, and J. M. Gambetta, *Nature* **549**, 242 (2017).

[33] C. Liu, H.-L. Huang, C. Chen, B.-Y. Wang, X.-L. Wang, T. Yang, L. Li, N.-L. Liu, J. P. Dowling, T. Byrnes, C.-Y. Lu, and J.-W. Pan, *Optica* **6**, 264 (2019).

[34] H.-L. Huang, M. Narożniak, F. Liang, Y. Zhao, A. D. Castellano, M. Gong, Y. Wu, S. Wang, J. Lin, Y. Xu, H. Deng, H. Rong, J. P. Dowling, C.-Z. Peng, T. Byrnes, X. Zhu, and J.-W. Pan, *Phys. Rev. Lett.* **126**, 090502 (2021).

[35] M. R. Geller, *Phys. Rev. Lett.* **127**, 090502 (2021).

[36] B. Nachman, M. Urbanek, W. A. de Jong, and C. W. Bauer, *npj Quantum Inf.* **6**, 84 (2020).

[37] S. Bravyi, S. Sheldon, A. Kandala, D. C. McKay, and J. M. Gambetta, *Phys. Rev. A* **103**, 042605 (2021).

[38] R. Hicks, B. Koirin, C. W. Bauer, and B. Nachman, arXiv:2108.12432 (2021).

[39] P. Das, S. Tannu, and M. Qureshi, in *MICRO '21*, MICRO '21 (Association for Computing Machinery, New York, NY, USA, 2021).

[40] S. S. Tannu and M. K. Qureshi, in *MICRO-52*, MICRO '52 (Association for Computing Machinery, New York, NY, USA, 2019) p. 279–290.

[41] J. Boyd, “Chebyshev & fourier spectral methods,” (2000) pp. 19–60.

[42] S. Ferracin, S. T. Merkel, D. McKay, and A. Datta, arXiv:2103.06603 (2021).

[43] H. Abraham *et al.*, “Qiskit: An open-source framework for quantum computing,” (2021).